HEMT DEVICE IN Ku BAND WITH III-As FOR SATELLITE APPLICATION

Z. KOURDI[a,*], M. KHAOUANI[b]
[a]*Ku team, Satellite development center, Algerian Space Agency, Oran, Algeria*
[b]*Faculty of technology, Tlemcen University, Tlemcen, Algeria*

In this work we focus in HEMTs (high electron mobility transistors) devices for can study all of the side effect by SILVACO-TCAD software. The structure shows a very good scalability in satellite domain applications especially in Ku band. That structure are with a short gate of 15 nm length are simulated, we exhibit an excellent current density as high with a value of 344 mA/mm, a cutting frequency of 285 GHz, a maximum frequency of 710 GHz, a maximum efficiency of 11%, a maximum breakdown voltage of 75 V. The hydrodynamics transporters are select in this simulation, and that physics model adopts for considering the accounts for the peculiarities of the GaAs material. A high accuracy for all relevant characteristics was achieved.

(Received April 1, 2020; accepted June 11, 2020)

Keywords: HEMT, Ku Band, Satellite, Tcad-Silvaco

1. Introduction

Today the satellite services are widely used for many sensitive and critical communications, the new space satellite constellations in the Ku-band satellite (GEO) becomes very interesting due to an increasing amount of transmitters and therefore lowered capacity costs.

Especially, the very small aperture terminals (VSAT) that ease the setup of a link are a growing market. Within the Ku-band, it has denoted the advantages of hybrid microwave integrated circuits in the Ku-band [1], [2].

The designing of circuits using in power amplifier application, requires accurate statistical models of the variations in the active device's performance that enable the designer to perform yield-oriented structure design of device.

III-As materials they provide promising advantages over the structures grown on GaAs substrates since they are less expensive, less fragile and available on a large scale. Meanwhile, efforts have been substantially devoted on the improvement of the performances such as instability and breakdown voltage.

It has been used to achieve long-term reliability and to act as an etch-stop layer in a selective-etch recessed-gate process, the composite or the doped channel [3] ,[4] has been used to overcome the small band gap energy of the InGaAs channel.

Aside from this, AlGaAs Schottky layer also induces a gate leakage issue, which causes the deterioration of device performance, especially when operating at higher bias conditions.

In HEMT device with InGaAs/AlGaAs/GaAs device, the undoped mince Schottky layer was used as with the gate Al2O3 passivation insulator layer with mode operating in a metal–insulator–semiconductor transistor [5], [6].

Therefore the passivation in gate and Si3N4 layer improvement in leakage current and breakdown voltage for can be surmounted oxide film as an insulator between the 2-D electron gas (2DEG) channel and the gate electrode, but also has the high density high-mobility 2DEG channel[7].

In this paper, we present with accurate the Ku-band internally-matched power amplifier, which uses a HEMT with III-As materials a thin film process for input and output matching circuits for Ku band..

* Corresponding author: zkourdi@hotmail.fr

2. Structure device

In this work, the III-As HEMT, which is simulated on a GaAs substrate with hydrodynamics model, has a 30 nm gate length and operates under Ku Band. Considering output matching loss, we chose this device for a Ku-band in power amplifier. A structure of this device its main performance parameters are shown in Fig. 1 and Table1.

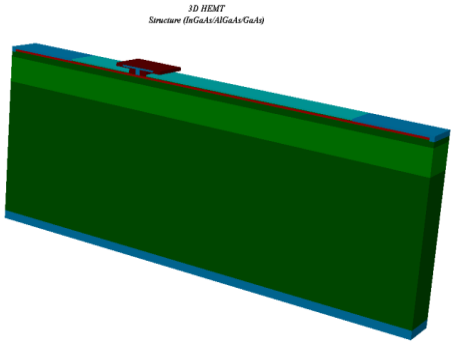

Fig. 1. 3D view of the structures HEMT Device.

Table 1. Materials and dopings of the different layers.

Layer	Material	Value
Cap	AlGaAs/GaAs	1xE21
Schottky	AlGaAs	NID
Donors	AlGaAs	1xE17
Spacer	AlGaAs	NID
Channel	InGaAs	1xE16
Buffer	AlGaAs	NID
Substrate	GaAs	NID

3. Results and discussion

3.1. DC analysis

For closer at the reality in our simulation we must carefully defining the Schottky contacts and interface states on the program.

The initial solution is calculated by taking the zero gate-source voltage (V_{GS} = 0 V) (initial declaration for the supply voltages). As the barrier is very thin, we use the hydrodynamic model.

We use the Gummel Newton method that must be declared for the calculation. In this case, if the solution does not converge in the framework of Gummel iterations, the program will automatically switch to Newton's algorithm.

The source and drain contacts are supposed to be ohmic. For the Schottky contact provided by the grid, the output work of the metal used is defined in the ATLAS input file. Ferthermore, contact declaration is necessary even if the material has already been used in the simulation. Since ATLAS does not recognize all metals, the value of the height of the Schottky barrier is introduced.

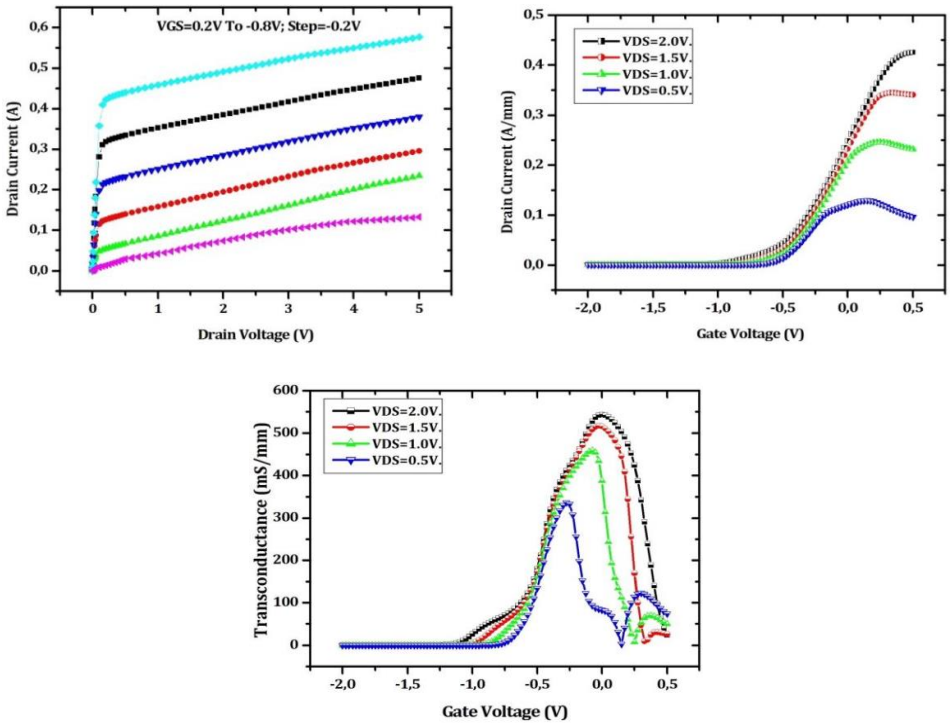

Fig. 2. Transfer characteristics, (b) output characteristics, (c) Transconductance characteristic.

FLDMOB makes it possible to activate the dependence of the mobility of the charge carriers on the field electric. CONMOB is specified for the concentration to be considered.

This is to simulate the output characteristics $I_{DS} = f(V_{DS})$ and transfer $I_{DS} = f(V_{GS})$.

We must take the drain voltage from 0 V to 5 V. This part of the simulation is performed using the method of Newton.

To simulate this characteristic; we vary the gate-source voltage (V_{GS}) from 0.2 V to - 0.8 V with a step of - 0.2 V. The result is represented in Fig. 2b. We have extract pinch voltage is -0.85 V.

For V_{GS} greater than or equal to zero volt, the elbow voltage is very small. The order of a R_{ON} resistor about 0.248 Ω.mm, between 0 and 0.3 V.

4.2. AC analysis

The Fig. 3, the pics for current gain (H_{21}), unilateral power gain (U_T), the maximum transducer gains power (GMT), stable maximum power gain (GMS) and available maximum power gain (GMA).

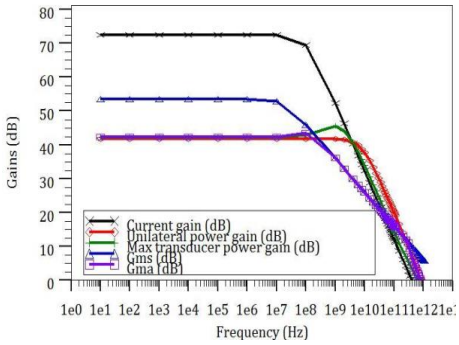

Fig. 3. Gains current gain, unilateral power gain, max transducer power gain (MTG) GMS and GMA versus frequency.

As observed from our results, the maximum gain shown for the current is 72 dB, the maximum transducer power gain, unilateral power gain and available maximum power gain are 42 dB, and the maximum stable power gain is 52 dB. The cutoff frequency for this device is 285 GHz, F_T is a boundary operating frequency in a device, the frequency response at which energy flowing through the device begins to be reduced rather than passing through, and we have extract a maximum frequency high 710 GHz.

4.3. RF analysis

The Fig. 4 shows the output power (Pout), power-added efficiency (PAE) and gain power (GP) versus the broad band RF performance over the 9–11 GHz frequency range at input power of 16 dBm.

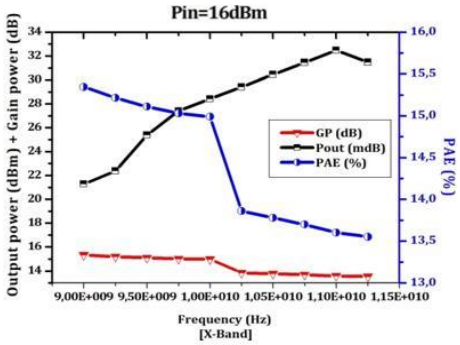

Fig. 4. Curves for power output, gain power and PAE versus frequency.

The simulated output power is 21 dBm (0.1258 W) at 9 GHz, and it achieves 33 dBm (~ 2 W) at 11 GHz. The gain power is around 15.1 dB between 9 GHz and 10 GHz; then it drops to less than 14 dB. The PAE is 15.3 % at 9 GHz; it is 15% at 10 GHz then it drops to about 13.5 % at 11.5 GHz.

So, compared these results with different precedent work as S. Piotrowicz and al.'s work [8] we can show a High efficiency in added power (PAE) at such polarization confirms the reduction of trapping effects in the devices.

It is essential for the operation of high-temperature transistors that is involved in power amplifiers.

4.4. Side effect analysis

4.4.1. Drain-Lag and Gate-Lag

The Fig. 5 (a shows gate lag effect can be traps responsible for the gate-lag are usually located below the gate. The interface between the semiconductor and the metallic contact must be of very good quality.

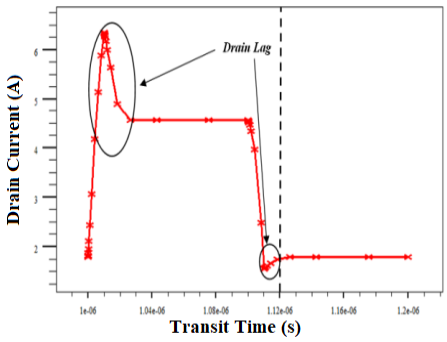

Fig. 5. Highlighting the Drain-Lag effect.

Indeed, when the gate voltage goes from the OFF state to the ON state, the output current takes several tens of microseconds to reach its established state in the usual structures: this is the transient behavior of the drain current. In our transistor, this time is of the order of the nanosecond.

The drain Lag can be calculating by:

$$G_{lag} = \frac{IDSS - IDSS0}{IDSS} \tag{1}$$

$$G_{lag} = \left[\frac{(1.59-1.54)}{1.59} + \frac{(1.78-1.74)}{1.78}\right]/_2 = 2.68\%$$

This phenomenon is related to the presence of traps in the semi-insulating substrate and at the surface in the gate-drain space during a rapid variation of the electric field between the drain and the source, the electrons from the channel can be trapped.

These electrons will be re-emitted with longer time constants. At the substrate level, the charge balancing then involves the appearance of a positively charged zone at the buffer-substrate interface in the buffer.

$$D_{Lag} = \left[\frac{(6.71-4.55)}{6.71} + \frac{(1.62-1.39)}{1.62}\right]/_2 = 23.14\% \tag{2}$$

4.4.2. Thermal effect

We illustrate at Fig. 6 the I_{DS}-V_{DS} characteristics for different temperature values: 250 K, 300 K, 350 K and 400 K.

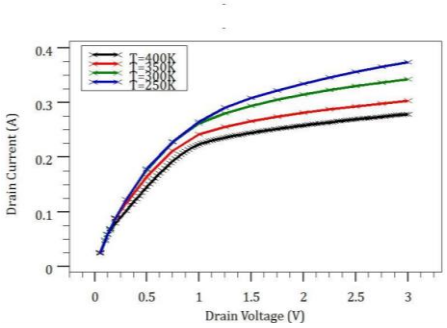

Fig. 6. Effect of temperature on I (V) characteristics.

The mobility of the charge carriers increases with the temperature. Furthermore, the electron-electron and electron-phonon interactions also increase, which decreases the output current. The phenomenon is clearly visible on simulated features. The slope of the IDS-VGS curve is practically constant; the temperature therefore has little influence on the control of the channel and the frequency of operation.

Self-heating effect

From the Fig. 7 we can shows the output characteristic self-heating of the studied structure; it is the evolution of the drain-source current (I_{DS}) as a function of the drain-source voltage (V_{DS}) at different values of the gate-source voltage (V_{GS}).

We vary the drain-source voltage from 0.0 to 5.0 V and the gate-source control voltage from 0 to -0.8 V.

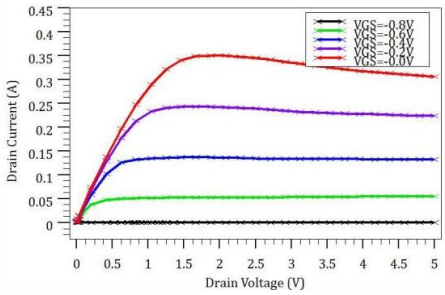

Fig. 7. Output characteristics of the HEMT studied with self-heating effect.

We obtain a maximum drain-source current (I_{DS}) of the order of 0.3 A. Owing to high operating voltage operation, self-heating effects should be to be take into consideration for our device. Self-heating effect is due to several various phenomena like the presence of surface traps in the semiconductor and raising the passivation layer thickness. Then, the choice of passivation material effectively influences the hot spot temperature [9].

5. Conclusion

Thanks to the interesting properties of the materials used, to the structure studied and also to the models and calculation methods of the software that we used to be as close as possible to reality. We accurate a very suitable value of D_{Lag} ,G_{Lag} of 23,14 %, 2,68 % Respectively and output power of 0.1258 W at 11 GHz and ~ 2 W at 9 GHz that we can said the results are according into literature results of this kind of devices and very valid. The most striking result is perhaps the performance that we obtained in this device would bring a lot to satellite application especially in Ku band.

References

[1] D. Maassen, F. Rautschke, F. Ohnimus, L. Schenk, U. Dalisda, G. Boeck: IEEE Transactions on Microwave Theory and Techniques. **65**(4), 1272 (2017).
[2] F. Rautschke, D. Maassen, F. Ohnimus, L. Schenk, U. Dalisda, G. Boeck, A hybrid 50-W GaN-HEMT Ku-band power amplifier, 46th European Microwave Conference (EuMC), p. 1079 (2016).
[3] T. Enoki, K. Arai, A. Kohzen, Y. Ishii, IEEE Trans. Electron Devices. **42**(8), 1413 (1995).
[4] J. A. del Alamo, T. Mizutani, IEEE Electron Device Lett. **10**(8), 394 (1989).
[5] H. Kinoshita, Y. Sano, T. Ishida, S. Nishi, M. Akiyama, K. Kaminishi, Jpn. J. Appl. Phys. **43**(11), L836 (1984).
[6] S. Fujita, M. Hirano, T. Mizutani, IEEE Electron Device Lett. **9**(10), 518 (1988).
[7] K-W. Lee, K. Lee, X. Lin, C. Tu, Y. Wang, IEEE Transactions On Electron Devices **54**(3), (2007).
[8] M. J. Uren, K. J. Nash, R. S. Balmer et al., IEEE Trans. Electron Devices. **53**, 395 (2006).
[9] Haghshenas, M. Fathipour, A. Mojab, Dependence of Self-heating Effect on Passivation Layer in AlGaN/GaN HEMT Devices, ISDRS, College Park, MD, USA, Dec 7–9,201.
[10] S. Piotrowicz, Z. Ouarch, E. Chartier, R. Aubry, G. Callet, D. Floriot, J. C. Jacquet, O. Jarde, E. Morvan, T. Reveyr, N. Sarazin, S. L. Delage, IEEE MTT-S International, p. 505 (2010).